# **Inorganic Chemistry**

pubs.acs.org/IC Article

# Rapid Cs<sup>+</sup> Capture via Multiple Supramolecular Interactions in Anionic Metal—Organic Framework Isomers

Kangwoo Jin, Xue-Qian Wu, Ying-Pin Chen, In-Hyeok Park, Jian-Rong Li,\* and Jinhee Park\*



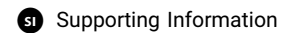
Cite This: Inorg. Chem. 2022, 61, 1918-1927



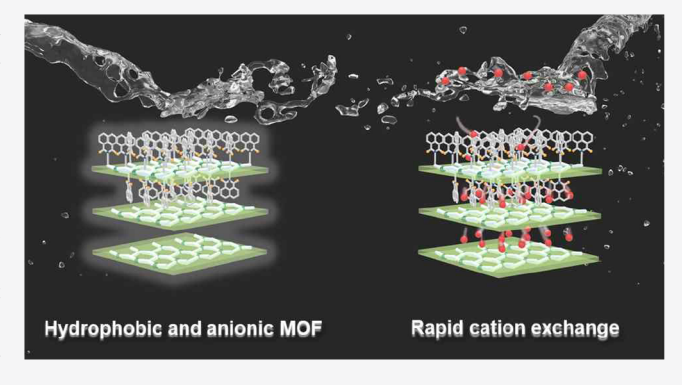
**ACCESS** I

Metrics & More





ABSTRACT: Metal—organic frameworks (MOFs) provide an ideal platform for ion exchange due to their high porosity and structural designability; however, developing MOFs that have the essential characteristics for ion exchange remains a challenge. These crucial features include fast kinetics, selectivity, and stability. We present two anionic isomers, DGIST-2 (2D) and DGIST-3 (3D), comprising distinctly arranged 5-(1,8-naphthalimido)-isophthalate ligands and In<sup>3+</sup> cations. Interestingly, in protic solvents, DGIST-2 transforms into a hydrolytically stable crystalline phase, DGIST-2'. DGIST-2' and DGIST-3 exhibit rapid Cs<sup>+</sup> adsorption kinetics, as well as high Cs<sup>+</sup> affinity in the presence of competing cations. The mechanism for rapid and selective sorption is explored based on the results of single-crystal



X-ray diffraction analysis of Cs<sup>+</sup>-incorporated DGIST-3. In Cs<sup>+</sup>-containing solutions, the loosely incorporated dimethylammonium countercation of the anionic framework is replaced by Cs<sup>+</sup>, which is held in the hydrophobic cavity by supramolecular ion—ion and cation— $\pi$  interactions.

### **■ INTRODUCTION**

Metal-organic frameworks (MOFs) comprise organic linkers and metal nodes connected by coordination bonds and have high porosities and versatile structures. Thus, numerous applications of MOFs, including adsorption, separation, and chemical sensing, have been reported in the last two decades.<sup>1-8</sup> However, the development of MOFs as ion exchange sorbents is challenging owing to the difficulty in preparing chemically stable ionic MOF systems. 9-11 Nonetheless, MOFs have high potential in this regard because of the following advantages: (i) high porosities and large surface areas that yield high sorption capacities, 12,13 (ii) an essentially infinite number of possible designs and tunable architectures that facilitate the introduction of binding sites for specific host-guest interactions, 14-16 and (iii) high crystallinity that enables precise structural analysis (via X-ray crystallography) and, thus, an in-depth understanding of the structure—property relationships. Crucially, structural analysis after ion adsorption can elucidate the sorption behavior and its associated

<sup>134/137</sup>Cs is a hazardous pollutant generated in the nuclear fuel cycle. Because of its similar chemical behavior to Na<sup>+</sup> or K<sup>+</sup>, Cs<sup>+</sup> can obstruct Na<sup>+</sup>/K<sup>+</sup> channels and accumulate in plant and animal tissues.<sup>22</sup> Consequently, Cs<sup>+</sup> easily enters the human body through the food chain, posing the risk of damaging the liver, kidneys, and the central nervous system.<sup>23</sup> Thus, it is important to capture radioactive Cs<sup>+</sup>. Various conventional techniques such as coagulation–flocculation–

settling, <sup>24</sup> liquid extraction, <sup>25</sup> and ion exchange <sup>26,27</sup> have been developed for this task. The ion exchange method is the most common approach because of its low cost, ease of operation, and low production of secondary waste. <sup>28,29</sup> To date, several ion exchange materials and related compounds such as polymer resins, <sup>30,31</sup> zeolites, <sup>32,33</sup> vanadosilicate, <sup>34</sup> metal chalcogenides, <sup>28,35–38</sup> ammonium phosphomolybdate—polyacrylonitrile (AMP–PAN), <sup>39,40</sup> crystalline silicotitanate (CST, IONSIV), <sup>41–43</sup> and hexacyanoferrates (Cstreat and Prussian blue) <sup>44,45</sup> have been developed.

However, studies that can establish the relationship between the adsorption properties and the structures of the ion exchangers have been rare. 46,47 This can be attributed to the slow adsorption kinetics 34 and the difficulties faced during structural analysis after Cs<sup>+</sup> adsorption. 34,35,48,49 Although several attempts for the removal of Cs<sup>+</sup> via ion exchange using MOFs have been reported, the lack of a driving force for Cs<sup>+</sup> adsorption and the high solvation energy of Cs<sup>+</sup> retard the Cs<sup>+</sup> removal from solution. 49–51 The slow sorption kinetics are problematic for column operation because the target ions

Received: September 29, 2021 Published: January 19, 2022





cannot be removed sufficiently rapidly under the conditions of fast flow rates, thus requiring large bed volumes. In addition, some MOFs collapse upon exposure to water. In addition, some MOFs collapse upon exposure to water. Strategies to achieve hydrolytic stability include the use of high-oxidation-state metal ions to increase coordination bond inertness and the introduction of bulk hydrophobic groups, such as long alkyl chains, on the organic linkers. However, for the former approach, sufficiently large single crystals required for structural analysis are usually difficult to obtain due to the poor reversibility of the coordination bonds. Meanwhile, the latter approach reduces the accessible pore volume, resulting in low surface area and functionality, thereby reducing the adsorption capacity.

In this study, we prepared an anionic  $In^{3+}$ -based MOF,  $[Me_2NH_2][In(\mathbf{L})_2]\cdot S_n$  ( $\mathbf{L}^{2-}=5$ -(1,8-naphthalimido)-isophthalate and S= pore-filling solvents), incorporating a multifunctional organic ligand. The hydrophobic nature of  $\mathbf{L}^{2-}$  can impart hydrolytic stability to the resulting MOF; it also creates hydrophobic cavities for the selective sorption of soft  $Cs^+$ . The electron-rich naphthyl group enables a cation- $\pi$  interaction with  $Cs^+$ . The cooperative supramolecular interactions including ion—ion and cation- $\pi$  interactions facilitate rapid  $Cs^+$  uptake. Although a few MOFs constructed from  $\mathbf{L}^{2-}$  have been reported to date,  $^{60,61}$  a combination of  $\mathbf{L}^{2-}$  and  $In^{3+}$  has not been reported, and adsorption-related applications have not been demonstrated.

### **■ EXPERIMENTAL SECTION**

**Materials.** Strontium chloride hexahydrate (SrCl<sub>2</sub>·6H<sub>2</sub>O, 99%) was purchased from Sigma-Aldrich. 1,8-Naphthalic anhydride (97%), 5-aminoisophthalic acid (95%), indium nitrate hydrate (In(NO<sub>3</sub>)<sub>3</sub>· xH<sub>2</sub>O, 99.99%), magnesium nitrate hexahydrate (Mg(NO<sub>3</sub>)<sub>2</sub>·6H<sub>2</sub>O, 99.99%), N,N-dimethylformamide (DMF, 99.8%), nitric acid (HNO<sub>3</sub>, 99.999%), tetrafluoroboric acid (HBF<sub>4</sub>, 50%), and calcium acetate hydrate (Ca(COOCH<sub>3</sub>)<sub>2</sub>·H<sub>2</sub>O, 99%) were purchased from Alfa Aesar. Cesium chloride (CsCl, 99%) was purchased from Tokyo Chemical Industry. Methyl alcohol (methanol, 99.99%) was purchased from B&J. Anhydrous potassium carbonate (K<sub>2</sub>CO<sub>3</sub>, 99.5%), sodium chloride (NaCl, 99%), dimethyl sulfoxide (DMSO, 99.5%), anhydrous ethyl alcohol (ethanol, 99.9%), and sodium hydroxide beads (NaOH, 98%) were purchased from Daejung Chemicals. All commercial chemicals were used without further purification.

Characterization. A proton nuclear magnetic resonance (<sup>1</sup>H NMR) spectrum was measured on an AVANCE III 400 Fourier transform NMR spectrometer (Bruker). Chemical shifts are reported in ppm downfield from DMSO- $d_6$  ( $\delta$  = 2.50). Field emission scanning electron microscopy (FE-SEM) and electron dispersive X-ray (EDX) images were collected using an S-4800 (Hitachi Ltd.). Single-crystal X-ray diffractometry (SXRD) was performed using a D8 Venture from Bruker and synchrotron radiation at the Pohang Accelerator Laboratory Beamline. Powder X-ray diffraction (PXRD) data were obtained with an Empyrean X-ray diffractometer (Panalytical). Contact angle measurement data were measured with a DCA-200A (Surface Electro-Optics). Distilled water was obtained from a Milli-Q Advantage A10. Inductively coupled plasma-mass spectrometry (ICP-MS) data were obtained with an iCAP Q ICP-MS (Thermo Scientific). Fourier transform-infrared (FT-IR) spectra were collected with a Nicolet Continuum infrared microscope (Thermo Scientific) in attenuated total reflectance (ATR) mode. Thermogravimetric analysis (TGA) data were obtained with an Auto Q500 (TA Instruments) with a heating rate of 2 °C/min to 300 and 10 °C/min to 800 °C. Elemental analysis (EA) was performed on a Vario MICRI Cube

**Synthesis of H<sub>2</sub>L.** H<sub>2</sub>L was synthesized according to a previously reported procedure with slight modifications. <sup>60</sup> 1,8-Naphthalic anhydride (6.129 g, 30.0 mmol) and 5-aminoisophthalic acid (6.865

g, 36.0 mmol) were added to DMF (360 mL) under inert conditions. The solution was heated under reflux and stirred overnight. The mixture then was cooled in the ice bath, and the resulting precipitate was filtered and washed with DMF several times. The cream colored product was placed in a flask, and a solution of methanol (150 mL) containing triethylamine (7.6 mL, 54.7 mmol) was added to the flask. The solution was stirred for 1 h. Then, insoluble impurities were removed by filtration, and the remaining homogeneous brown solution was acidified with 3 M HCl (100 mL). The precipitate was collected and washed with water and methanol. The neutralized white solid was dried in vacuo (23.1 mmol, 8.3 g, and yield 77.0%).

**Synthesis of DGIST-2.** A solid mixture of  $\dot{H}_2L$  (1000 mg, 2.77 mmol) and  $In(NO_3)_3$ : $xH_2O$  (222.2 mg, 0.74 mmol) was dissolved in a mixture of DMF/DMSO (1.0:1.0 v/v, 400 mL) in a 500 mL lab bottle before water (20 mL) was added to the solution. The lab bottle was capped and heated at 120 °C for 3 days, after which time, colorless polyhedral crystals of DGIST-2 ([Me<sub>2</sub>NH<sub>2</sub>][In(L)<sub>2</sub>]·S<sub>n</sub>) were obtained (0.499 g and 76.8% yield based on In).

Syntheses of DGIST-3-S, DGIST-3-M, and DGIST-3-L. A solid mixture of  $H_2L$  (1000 mg, 2.77 mmol) and  $In(NO_3)_3\cdot xH_2O$  (222.2 mg, 0.74 mmol) was dispersed in DMF (400 mL) in a 500 mL lab bottle before varying amounts of water were added. To obtain DGIST-3-S and DGIST-3-M, water (30 and 23 mL, respectively) was added to the dispersion. To obtain DGIST-3-L, water (23 mL) and HBF<sub>4</sub> (2 mL) were added to the turbid solution. The lab bottle was capped and heated at 100 °C for 3 days, after which time, colorless polyhedral crystals of DGIST-3 ([Me<sub>2</sub>NH<sub>2</sub>][In(L)<sub>2</sub>]·S<sub>n</sub>) were obtained (0.523 g and 80.5% yield for DGIST-3-S, 0.566 g and 87.0% yield for DGIST-3-M, and 0.495 g and 76.2% yield for DGIST-3-L—the yields were calculated based on In).

Cs<sup>+</sup>@DGIST-3 Single Crystals. A solid mixture of  $H_2L$  (10.0 mg, 0.03 mmol) and  $In(NO_3)_3$ : $xH_2O$  (4.4 mg, 0.02 mmol) was dissolved in a mixture of DMF/DMSO (1.0:1.0 v/v, 4 mL) in a vial, and then 0.23 mL of water was added to the mixture. The vial was capped and heated at 80 °C. After 5 days, single crystals of mixed phases of DGIST-2 and DGIST-3 were obtained. The resultant crystals were washed with fresh DMF and methanol several times and then stored in a 50 mM CsCl solution in methanol for 1 day (11.6 mg and 90.0% yield based on In).

Mass Calibration of Adsorbents. The air-dried powders used for Cs<sup>+</sup> adsorption contained residual solvents. To accurately measure the adsorption capacity, the exact adsorbent mass without any residual solvent is required. Concentrated HNO<sub>3</sub> was added to dissolve the air-dried MOF powder. The dissolved solution was diluted with a 0.1 wt % aqueous HNO<sub>3</sub> solution to obtain the concentration required for ICP-MS. Further, ICP-MS revealed the concentration of In<sup>3+</sup> in the diluted solution. The exact adsorbent mass was calculated using eqs 1 and 2

$$In^{3+}_{m} = \frac{concn \text{ of } In^{3+}(ppm) \times total \text{ amounts of diluted soln}(g)}{10^{6}} \times 10^{3}$$
(1)

$$M = \frac{\text{formula weight of an MOF (879.5 g/mol)}}{\text{atomic weight of In (114.8 g/mol)}} \times \text{In}^{3+}_{\text{m}}$$
 (2)

where  $In^{3+}_{m}$  is the amount of  $In^{3+}$  (mg), and M is the amount of activated adsorbent (mg).

**Theoretical Ion Exchange Capacity.** Theoretical ion exchange capacity was calculated according to a previously reported equation: <sup>49</sup>

$$q(theoretical) = \frac{\text{atomic weight of cesium}}{\text{formula weight of a MOF}} \times 10^3 = \frac{132.9}{879.5} \times 10^3$$
$$= 151.1 \text{ mg g}^{-1}$$
(3)

Cs<sup>+</sup> Adsorption Kinetics Test for DGIST-2′⊃methanol in Methanolic Solutions. The as-synthesized DGIST-2 crystals were washed several times with DMF and exchanged with methanol to prepare DGIST-2′⊃methanol. Wet DGIST-2′⊃methanol crystals (adsorbent mass = 82.8 mg) were placed in a 250 mL lab bottle,

and pure methanol was added until the total weight of the solutions was approximately 20 g. Then, 80 g of a methanolic CsCl solution (144.4 ppm) was added, and the mixture was stirred magnetically. Aliquots (2 mL) were obtained at different contact times (1, 5, 15, 60, and 180 min). The obtained Cs⁺@DGIST-2′⊃methanol crystals were immediately washed several times with fresh methanol, and concentrated HNO₃ was added to dissolve Cs⁺@DGIST-2′⊃methanol. The dissolved solutions were diluted with 0.1 wt % aqueous HNO₃ solutions to obtain the concentration required for ICP-MS measurement. The exchange capacities (q, mg g⁻¹) of DGIST-2′⊃methanol were calculated using eqs 1−5

$$Cs_{m}^{+} = \frac{\text{concn of } Cs^{+}(\text{ppm}) \times \text{total amounts of dissolved soln}(g)}{10^{6}} \times 10^{3}$$
(4)

$$q = \frac{\mathrm{Cs^+}_{\mathrm{m}}}{\mathrm{M}} \tag{5}$$

where  $\operatorname{Cs^+}_m$  and  $\operatorname{In^{3+}}_m$  are the amounts of adsorbed  $\operatorname{Cs^+}$  (mg) and  $\operatorname{In^{3+}}$  (mg), respectively, and M is the amount of adsorbent, viz., DGIST-2′ (g), at different contact times.

Cs<sup>+</sup> Adsorption Kinetics Tests for DGIST-3-S, DGIST-3-M, and DGIST-3-L in Methanolic Solutions. The as-synthesized DGIST-3-S, DGIST-3-M, and DGIST-3-L crystals were washed several times with DMF and dried in air for 12 h. Then, air-dried DGIST-3-S, DGIST-3-M, and DGIST-3-L crystals (adsorbent mass = 94.4 mg) were placed in sealed 250 mL lab bottles, and pure methanol was added until the total weight of the solutions reached approximately 20 g. To these solutions, 80 g of methanolic CsCl solutions (≈170 ppm) was added, and the mixtures were stirred magnetically. Aliquots (2 mL) were extracted at different contact times (1, 5, 15, 60, and 180 min). The extracted solutions were filtered through a 0.20- $\mu$ m DISMIC filter and diluted with 0.1 wt % aqueous HNO3 solutions to obtain the concentration required for ICP-MS measurement. The kinetic curves were plotted as a function of contact time. The exchange capacities  $(q, \text{ mg g}^{-1})$  of DGIST-3-S, DGIST-3-M, and DGIST-3-L were calculated using eq 6

$$q = \frac{(C_0 - C_t)M_s}{m} \tag{6}$$

where  $C_0$  and  $C_t$  (ppm) are the initial and equilibrium concentrations of  $\mathrm{Cs}^+$ , respectively, m (mg) is the mass of the sorbent, and  $M_{\mathrm{s}}$  (g) is the mass of the solution.

Cs<sup>+</sup> Adsorption Kinetics Tests for DGIST-2′⊃water in Aqueous Solutions. The as-synthesized DGIST-2 crystals were washed with DMF and ethanol several times and dried in air for 12 h. Dried DGIST-2′⊃ethanol powders were placed in sealed 250 mL lab bottles, and pure water was added until the total weight of the solutions reached approximately 20 g. Then, 80 g of an aqueous CsCl solution (146.6 ppm) was added, and the mixture was stirred magnetically. Aliquots (2 mL) were extracted at different contact times (1, 5, 15, and 60 min), and the extracted solutions were filtered through a 0.20-µm DISMIC filter and diluted with 0.1 wt % aqueous HNO<sub>3</sub> solutions to obtain the concentration required for ICP-MS measurement. The kinetic curves were plotted as a function of contact time. The exchange capacities (q, mg g<sup>-1</sup>) of DGIST-2′⊃water were calculated using eq 6.

**Pseudo Kinetic Models.** The data obtained from the kinetics experiments were fitted by two pseudo-first-order and pseudo-second-order kinetic models, which are described in eqs 7 and 8, respectively.

$$In(q_e - q_t) = In(q_e) - k_1 t \tag{7}$$

$$\frac{t}{q_t} = \frac{1}{k_2 q_o^2} + \frac{1}{q_o} t \tag{8}$$

Here, t is the adsorption time (min),  $q_{\rm e}$  and  $q_t$  are the amounts of adsorbed Cs<sup>+</sup> (mg g<sup>-1</sup>) at equilibrium and at time t, respectively, and  $k_1$  (min<sup>-1</sup>) and  $k_2$  (g mg<sup>-1</sup> min<sup>-1</sup>) are the pseudo-first-order and pseudo-second-order rate constants of adsorption, respectively.

Cs<sup>+</sup> Adsorption Isotherm Tests for DGIST-2′⊃methanol and DGIST-3-S in Methanolic Solutions. Different amounts of CsCl were dissolved in methanol to perform batch experiments. The airdried DGIST-2 and DGIST-3-S powders (adsorbent mass = 11.8 mg) were added to a glass vial containing 10 mL of a  $Cs^+$  solution (adsorbent dosage = 1.18 g  $L^{-1}$ ), and the mixtures were stirred for 5 h at room temperature. During this process, air-dried DGIST-2 was completely transformed into Cs<sup>+</sup>@DGIST-2′⊃methanol. The resultant solutions were centrifuged to isolate Cs<sup>+</sup>@DGIST-2′⊃methanol and Cs<sup>+</sup>@DGIST-3-S. The isolated powders were washed several times with fresh methanol and were dried under vacuum. Concentrated HNO3 was added to the dried powders, and the dissolved solutions were diluted with 0.1 wt % aqueous HNO3 solutions. The amounts of In and Cs in the solutions were determined by ICP-MS experiments. The amount of adsorbed Cs<sup>+</sup> (q, mg g<sup>-1</sup>) was calculated according to eqs 1-5. All the experiments were performed at room temperature and repeated three times to confirm the reproducibility of the data. The Langmuir and Langmuir-Freundlich models are described in eqs 9 and 10, respectively.

$$q = q_{\rm m} \frac{bC_e}{1 + bC_e} \tag{9}$$

$$q = q_{\rm m} \frac{bC_{\rm e}}{1 + (bC_{\rm e})^{1/n}} \tag{10}$$

Here, q (mg g<sup>-1</sup>) and  $q_m$  (mg g<sup>-1</sup>) are the amounts of Cs<sup>+</sup> adsorbed at  $C_e$  and the maximum Cs<sup>+</sup> adsorption capacity, respectively, b (L mg<sup>-1</sup>) is the Langmuir constant related to the free energy of the exchange, and n is a constant characterizing the system heterogeneity.

Cs<sup>+</sup> Adsorption Isotherm Tests for DGIST-2' in Aqueous **Solutions.** Different amounts of CsCl were dissolved in water to perform batch experiments. Air-dried DGIST-2'Dethanol powders (adsorbent mass = 11.8 mg) were added to a glass vial containing 10 mL of a  $Cs^+$  solution (adsorbent dosage = 1.18 g  $L^{-1}$ ), and the mixtures were stirred for 5 h at room temperature. During this process, air-dried DGIST-2 was completely transformed into Cs+@ DGIST-2'Dwater. The resultant solutions were centrifuged to isolate Cs<sup>+</sup>@DGIST-2′⊃water. The isolated powders were washed several times with fresh methanol and dried under vacuum. Concentrated HNO<sub>3</sub> was added to the dried powders, and the dissolved solutions were diluted with 0.1 wt % aqueous HNO3 solutions. The amounts of In and Cs in the solutions were determined by ICP-MS experiments. The amount of adsorbed  $Cs^+$   $(q, mg g^{-1})$  was calculated according to eqs 2-5. All the experiments were performed at room temperature and repeated three times to confirm the reproducibility of the data.

Cs<sup>+</sup> Adsorption Selectivity Tests. Approximately 1 ppm solutions of Cs<sup>+</sup> (0.00596 mmol) and a mixture of 10 times molar excesses of Na<sup>+</sup>, K<sup>+</sup>, Mg<sup>2+</sup>, Ca<sup>2+</sup>, and Sr<sup>2+</sup> in methanol (10 mL) were added to air-dried DGIST-2 and DGIST-3-S crystals (adsorbent = 11.8 mg) in a 20 mL vial followed by stirring for 5 h at room temperature. During this process, air-dried DGIST-2 was completely transformed into Cs<sup>+</sup>@DGIST-2′ $\supset$ methanol. The resulting solutions were filtered through a 0.20- $\mu$ m DISMIC filter and diluted with 0.1 wt % aqueous HNO<sub>3</sub> solutions to obtain the concentration required for ICP-MS measurement. The entire process was performed three times to confirm the reproducibility of the data. ICP-MS data were recorded to determine the Cs<sup>+</sup> removal efficiencies (%) as follows

$$Cs^{+} \text{ removal efficiency (\%)} = \frac{|C_f - C_0|}{C_0} \times 10^2$$
(11)

where  $C_f$  is the concentration of Cs<sup>+</sup> after 5 h, and  $C_0$  is the initial concentration of Cs<sup>+</sup> in methanol.

#### RESULTS AND DISCUSSION

**Structures of DGIST-2 and DGIST-3.** Two anionic MOF isomers of  $[Me_2NH_2][In(L)_2]\cdot S_n$ , having 2D and 3D architectures, denoted as DGIST-2 and DGIST-3, respectively, were obtained from the solvothermal reaction of  $H_2L$  and

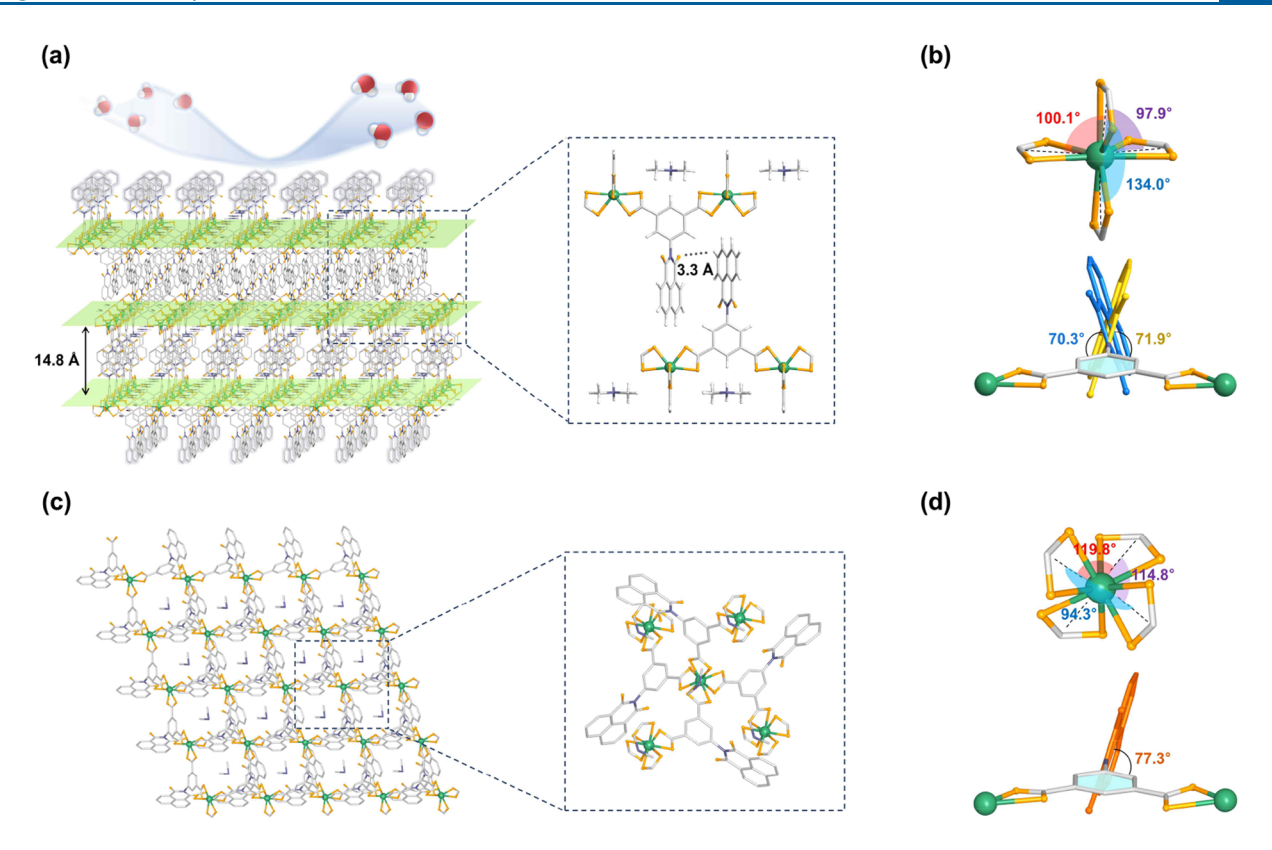


Figure 1. (a) Layered structure of DGIST-2 and its hydrophobic nature. (Inset)  $C-H\cdots O$  hydrogen bonds between neighboring layers. (b) Coordination bond angles of  $In(COO)_4^-$  nodes and dihedral angles of  $L^{2-}$  in DGIST-2. (c) View of the 3D crystal structure of DGIST-3. (Inset) 3D coordination environment of DGIST-3. (d) Coordination bond angles of  $In(COO)_4^-$  nodes and a dihedral angle of  $L^{2-}$  in DGIST-3. Green, In; yellow, O; gray, C; blue, N; and white, H. Hydrogen atoms are omitted for clarity.

 $In(NO_3)_3$ . The structures of DGIST-2 and DGIST-3 were determined by SXRD and were shown to contain a mononuclear node  $(In(COO)_4^-)$ , in which  $In^{3+}$  was coordinated to four carboxylates derived from four  $L^{2-}$  ligands (Figures 1a and 1c). Furthermore, exchangeable  $[Me_2NH_2]^+$  ions (from hydrolyzed DMF) were incorporated into the anionic frameworks,  $[In(L)_2]^-$ , to achieve charge balancing.

In DGIST-2 (monoclinic, I2/a space group), the building units are connected to form 2D square grid networks, and the naphthalimide moieties of  $L^{2-}$  along the *c*-axis show positional disorder. The distance between the O (O5Y) of the imide group and H (H14Y) of the naphthyl group from another sheet is approximately 3.28 Å, suggesting 3D network formation via C-H···O hydrogen bonds (Figure 1a). In DGIST-3 (orthorhombic, Fdd2 space group), the nodes and L<sup>2-</sup> form a 3D structure (Figure 1c). The structures of DGIST-2 and DGIST-3 differ in terms of the coordination angles of the  $In(COO)_4^-$  node. The C-In-C angles in DGIST-2 are 97.9°, 100.1°, and 134.0°, whereas those in DGIST-3 are 94.3°, 114.8°, and 119.8° (Figures 1b and 1d). The PXRD patterns of as-synthesized DGIST-2 and DGIST-3 match the simulated patterns obtained from the single-crystal structures, confirming the phase purity (Figures 2a and 2e).

Structural Transformation and Stability. Interestingly, when DGIST-2, immersed in DMF, was solvent-exchanged with ethanol, it was transformed into a new phase within 5 min (Figure 2a). Similar transformations to this new phase were also observed in other polar protic solvents such as methanol and water (Figure 2b). Although the structure of DGIST-2 was lost upon drying, air-dried DGIST-2 regenerated into the new

phase within 5 min in ethanol (Figure S9). The DGIST-2 phase obtained after immersion in water, ethanol, or methanol for 5 h is labeled as DGIST-2' $\supset$ water, DGIST-2' $\supset$ ethanol, and DGIST-2' $\supset$ methanol, respectively. Although a complete SXRD analysis was not possible owing to the deteriorated crystallinity, DGIST-2' $\supset$ ethanol was preserved in relatively good condition. Hence, the 2D layered structure of DGIST-2' $\supset$ ethanol was elucidated based on the diffraction peaks. Importantly, the distance between the 2D layers reduced from 14.8 to 13.4 Å during this phase transition, as evidenced by the PXRD analysis. The peak at  $2\theta = 6.0^{\circ}$ , corresponding to the (004) reflection plane, shifted to a higher angle ( $2\theta = 6.6^{\circ}$ ).

DGIST-2'⊃water was moderately stable in aqueous solutions across a pH range of 3-11 over 3 days (Figure 2d). However, after immersion in water for 2 h, the morphology of DGIST-3 changed, whereupon its crystallinity was lost (Figure 2e). Contact angle measurements of the DGIST-2′Dethanol and DGIST-3 powders were conducted using the Washburn method. 62 Intriguingly, despite the presence of In(COO)<sub>4</sub> sites, the advancing water contact angles were 81.4° and 76.8° for DGIST-2′⊃ethanol and DGIST-3, respectively, higher than the values recorded for typical MOFs. 63-65 This difference in the water contact angles of the two MOFs can be attributed to the different functional groups on the crystal surfaces; that of DGIST-3 is mainly terminated by hydrophilic carboxylic acid or carboxylate groups of HL<sup>-</sup> and formate (Figure 1c), while that of DGIST-2 is terminated by hydrophobic naphthyl moieties (Figure 1a), which confer hydrolytic stability. In addition, in the phase transition of DGIST-2, the accessibility of the

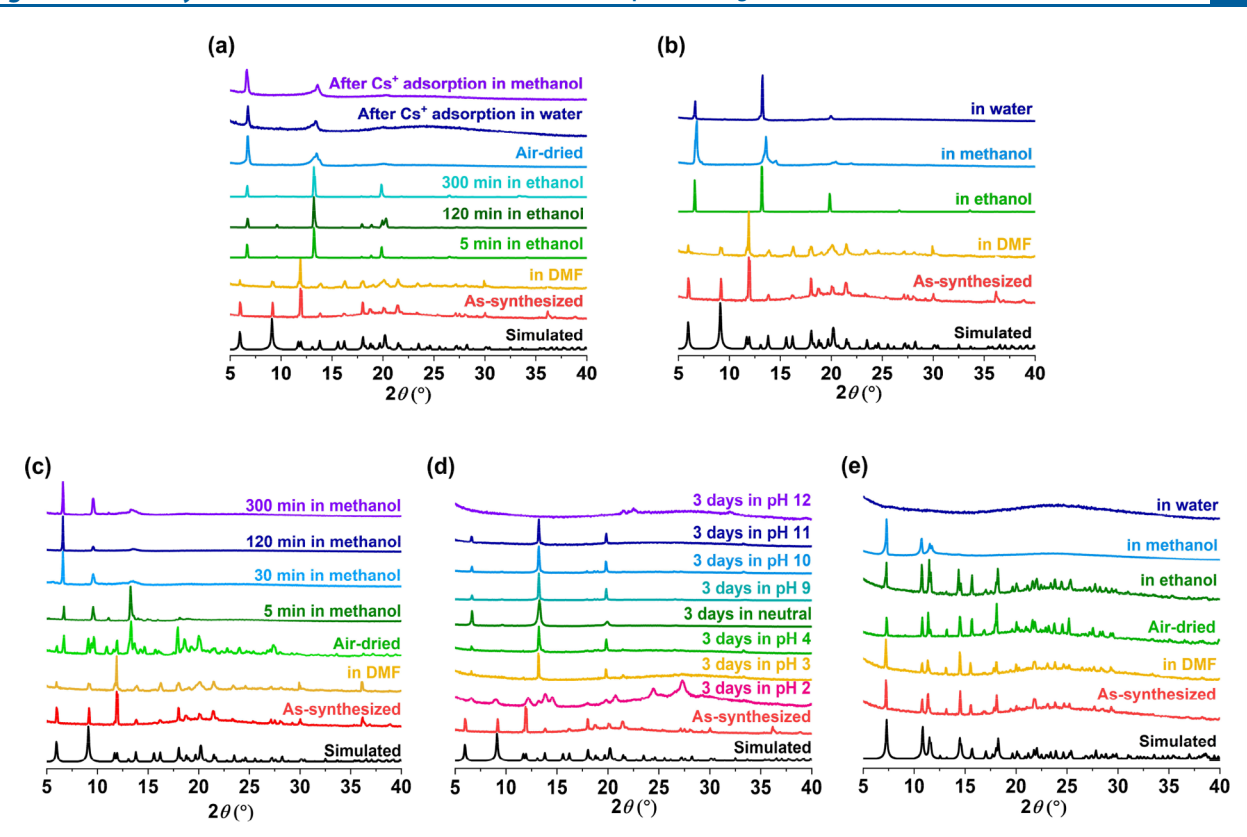


Figure 2. PXRD patterns of (a) DGIST-2 simulated, as-synthesized, soaked in DMF, after soaking in ethanol for 5, 120, and 300 min, air-dried, and after Cs<sup>+</sup> adsorption in water and methanol; (b) DGIST-2 simulated, as-synthesized, soaked in DMF, DGIST-2'Dethanol, DGIST-2'Dethanol, and DGIST-2'Dwater; (c) DGIST-2 simulated, as-synthesized, soaked in DMF, air-dried, and air-dried after soaking in methanol for 5, 180, and 300 min; (d) DGIST-2 simulated, as-synthesized, and after exposure to pH 2–12 solutions for 3 days; and (e) DGIST-3-S simulated, as-synthesized, soaked in DMF, air-dried, and after exposure to ethanol, methanol, and water.

 $In(COO)_4^-$  sites is hindered by the naphthyl moieties due to the shorter interlayer distance, which further inhibits the approach of the water molecules. In fact, some  $In^{3+}$  clusters, such as trinuclear  $In_3(\mu_3\text{-O})(COO)_6^{66,67}$  or  $[In(OH)-(COO)_2]_n$  chains,  $^{68-71}$  are known to be hydrolytically stable. However, despite their facile synthesis and useful anionic nature, the stability of eight-coordinate monomeric  $In^{3+}$ -based MOFs is not guaranteed.  $^{72-78}$  Apart from those related to interpenetrating isomers, studies regarding the stability differences arising from ligand and metal arrangements, as observed in DGIST-2' and DGIST-3, have rarely been reported.  $^{71,79}$ 

Adsorption Kinetics Studies. The anionic nature of DGIST-2 and DGIST-3 prompted us to conduct Cs<sup>+</sup> exchange experiments. Because of its structural rigidity, air-dried DGIST-3 powder was used to obtain adsorption isotherms and kinetics (Figure 2e). Air-dried DGIST-2 was gradually transformed into DGIST-2′⊃methanol upon immersion in methanol (Figure 2c). Thus, the air-drying step should not affect the adsorption capacity if sufficient contact time is allowed for structural restoration. However, because kinetics experiments require short contact times, completely transformed DGIST-2′⊃methanol must be used; thus, DGIST-2′⊃methanol soaked in methanol for at least 5 h was used in such experiments.

The effects of the crystal size were investigated using DGIST-3 crystals of three different sizes, namely  $10-800~\mu m$  (DGIST-3-L),  $10-100~\mu m$  (DGIST-3-M), and  $5-30~\mu m$  (DGIST-3-S), which were synthesized by controlling the water content and using HBF<sub>4</sub> (Figures S4 and S5). The amount of

Cs<sup>+</sup> adsorbed as a function of the exposure time was determined by inductively coupled plasma-mass spectrometry. It was found that DGIST-3-S reached its maximum Cs<sup>+</sup> uptake capacity within 1 min. This is the shortest period for which reliable kinetic data can be obtained (Figure 3b and Table S10). Interestingly, despite their large crystallites ( $<800 \mu m$ ), DGIST-2'>methanol and DGIST-3-L exhibited rapid Cs+ uptakes in methanolic solutions, reaching equilibrium within 15 min (Figures 3a and 3b and Tables S9 and S10). The Cs<sup>+</sup> sorption kinetics of DGIST-2'>methanol and DGIST-3 showed the best fit with the pseudo-second-order kinetics model, indicating that chemisorption is the rate-determining step (Figures S12-S15, Tables S13 and S14).80 Chemical adsorption is based on much stronger interactions than those entailed in physical adsorption. The interactions in chemical adsorption involve the sharing of electrons between the adsorbate and adsorbent surface. Hence, most Cs<sup>+</sup> adsorbents involving ion-ion interactions are mathematically fitted to a pseudo-second-order kinetic model. 49,81,82 The slight increase in the adsorption capacity of DGIST-3 with a decrease in the particle size may be due to the relatively larger surface area to volume ratios of the smaller particles.

**Adsorption Isotherm Studies.** Adsorption isotherms of DGIST-2' $\supset$ methanol and DGIST-3-S were fitted to the Langmuir–Freundlich model (Figures 3d and 3e and Tables S16 and S17), and the calculated maximum adsorption capacities were 183  $\pm$  15 and 156  $\pm$  7 mg g<sup>-1</sup>, respectively. These values are similar to the theoretical capacity of 151.1 mg g<sup>-1</sup>. Thus, it can be inferred that the structural transformation

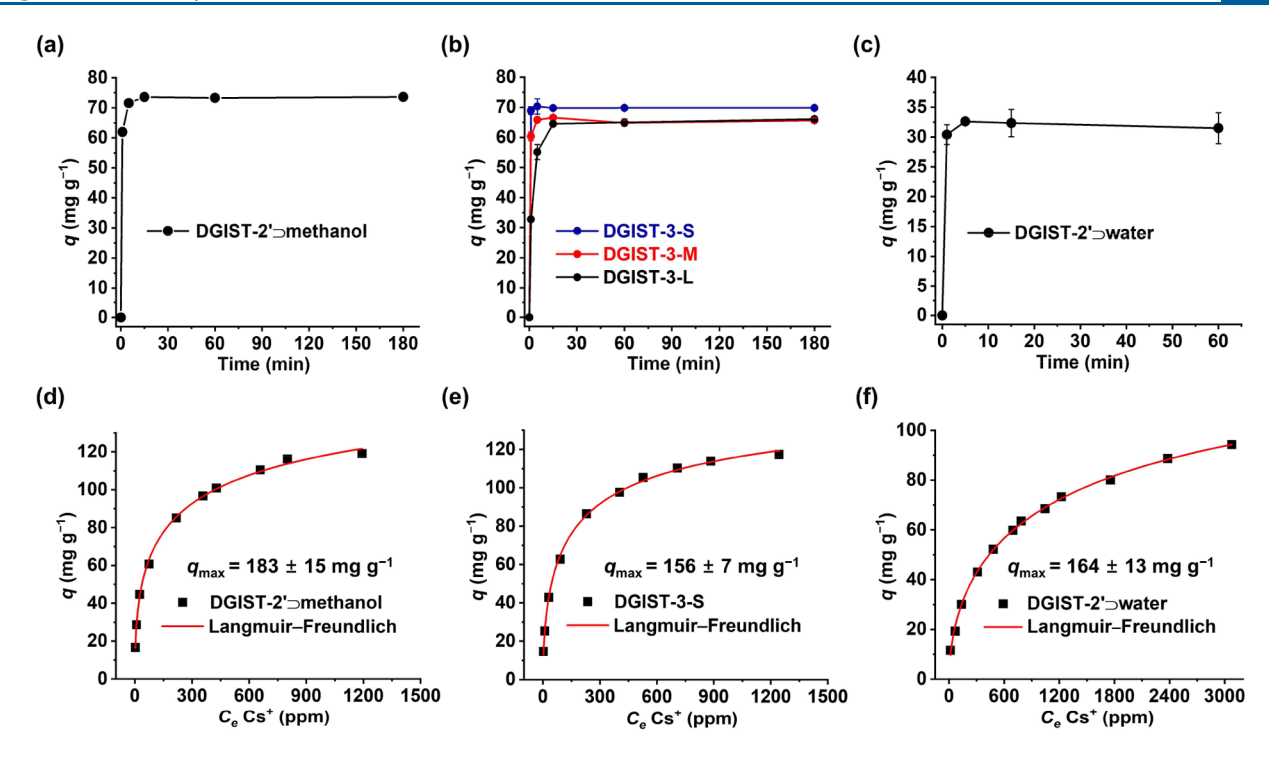


Figure 3. Kinetics of Cs<sup>+</sup> exchange in methanolic solutions for (a) DGIST-2' $\supset$ methanol (initial [Cs<sup>+</sup>] = 115 ppm and adsorbent dose = 0.66 g L<sup>-1</sup>) and (b) DGIST-3-N, and DGIST-3-L (initial [Cs<sup>+</sup>]  $\approx$  130 ppm and adsorbent dose = 0.75 g L<sup>-1</sup>). (c) Cs<sup>+</sup> adsorption kinetics in an aqueous solution for DGIST-2' $\supset$ water (initial [Cs<sup>+</sup>] = 117 ppm and adsorbent dose = 0.74 g L<sup>-1</sup>). Cs<sup>+</sup> adsorption isotherms in methanolic solutions: (d) DGIST-2' $\supset$ methanol and (e) DGIST-3-S (equilibrium concentrations in the range of 2–1244 ppm, adsorbent dose = 1.18 g L<sup>-1</sup>, and contact time = 5 h). (f) Cs<sup>+</sup> adsorption isotherm of DGIST-2' $\supset$ water (equilibrium concentration range = 15–3077 ppm, adsorbent dose = 1.18 g L<sup>-1</sup>, and contact time = 5 h).

from DGIST-2 to DGIST-2′⊃methanol does not reduce the sorption capacity, and the In(COO)<sub>4</sub><sup>-</sup> sites in DGIST-2′⊃methanol remain available for cation adsorption. Energy-dispersive X-ray mapping analysis of Cs<sup>+</sup>-containing DGIST-2′⊃methanol and DGIST-3-M revealed that a substantial amount of Cs (comparable to that of In) was uniformly dispersed throughout the crystals (Figure S8). These sorption capacities are higher than or comparable to those of Cstreat (32 mg g<sup>-1</sup>),<sup>44</sup> AMP−PAN (81 mg g<sup>-1</sup>),<sup>39</sup> and CST (186 mg g<sup>-1</sup>),<sup>42</sup> commercially available Cs<sup>+</sup> scavengers, that require many minutes or even hours to attain their maximum capacities.<sup>34</sup> For easy comparison, Table S18 lists the adsorption performance characteristics of the various sorbents.

DGIST-2'Dwater is hydrolytically stable, enabling the examination of its Cs<sup>+</sup> adsorption in water. Dried DGIST-2'Dethanol was used to minimize the release of the organic solvent molecules during Cs<sup>+</sup> exchange in water. Promisingly, once DGIST-2 is transformed into DGIST-2'Dethanol, the airdrying step does not significantly alter the structure (Figure 2a). Interestingly, the Cs<sup>+</sup> uptake in an aqueous solution was faster than that in the methanolic solution. Most of the Cs+ uptake occurred in the first 1 min, and equilibrium was reached within 5 min (Figure 3c and Table S19). In contrast to the crystal surface of DGIST-2'>methanol, that of DGIST-2'Dwater exhibited slight dimples, indicating the formation of defects in the crystals, as shown in Figure S7. Compared with a flat surface, such an indented surface with a large exposed surface area enables Cs<sup>+</sup> to more rapidly transport to the adsorption sites. It is worth noting that the defect formation in the case of water did not induce leaching of the ligand and In<sup>3+</sup>. Compared to other reported MOF sorbents

for Cs<sup>+</sup> (Table S18), the sorbents prepared in this study show the fastest uptake kinetics. Although the maximum Cs+ sorption capacity in water was slightly reduced to  $164 \pm 13$ mg g<sup>-1</sup>, this value is still comparable to the theoretical value (Figure 3f and Table S21). The Langmuir constant, which represents the adsorbate-adsorbent affinity, decreased from  $0.0035 \pm 0.001$  to 0.00055 L mg<sup>-1</sup> because the Cs<sup>+</sup> solvation energy in water is higher than that in methanol (Tables S15 and S21). This result is consistent with the lower sorption capacity (33 mg g<sup>-1</sup>) obtained in the kinetics experiments. Importantly, no released indium species were detected during Cs<sup>+</sup> adsorption in water. To examine the effect of pH on the adsorption capacities, adsorption isotherms were obtained at pH 4 and 9 (Figure S19). The Cs<sup>+</sup> exchange experiments were not performed in strongly acidic (pH 3) and basic (pH 10) solutions because of the leaching of In3+ from DGIST-2'⊃water in the presence of Cs<sup>+</sup>. The maximum capacities at pH 4 and pH 9 were  $60 \pm 3$  and  $86 \pm 16$  mg g<sup>-1</sup>, respectively. These low capacities at pH 4 and pH 9, compared with those at pH 7 (164  $\pm$  13 mg g<sup>-1</sup>), were presumably because Cs<sup>+</sup> and H<sub>3</sub>O<sup>+</sup> compete with each other at pH 4 and OH<sup>-</sup> reduces the interaction of Cs<sup>+</sup> with the MOF at pH 9.

Competing Cation Effects. To investigate the effects of competing cations, Cs<sup>+</sup> adsorption experiments were conducted with a 10 times molar excess of Na<sup>+</sup>, K<sup>+</sup>, Mg<sup>2+</sup>, Ca<sup>2+</sup>, and Sr<sup>2+</sup>. The Cs<sup>+</sup> removal efficiencies of DGIST-2′⊃methanol and DGIST-3 were 87.4% and 90.0%, respectively, slightly lower than the 98.0% and 98.2% efficiencies, respectively, in the absence of competing ions (Figure 4a and Table S24). The Cs<sup>+</sup> selectivity can be attributed to the hydrophobic cavities in DGIST-2′⊃methanol and DGIST-3 that preferentially ad-

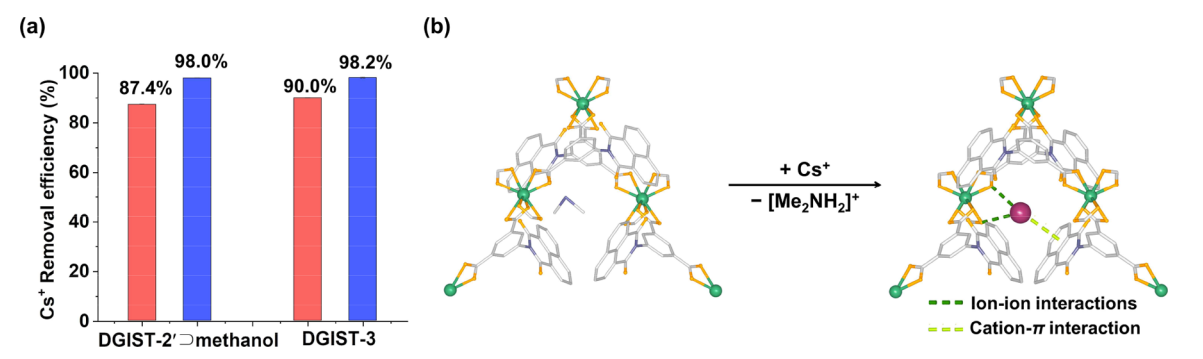


Figure 4. (a) Competing ion experiments for DGIST-2′ $\supset$ methanol and DGIST-3. Red bars represent Cs<sup>+</sup> removal efficiency (%) in the presence of Na<sup>+</sup>, K<sup>+</sup>, Mg<sup>2+</sup>, Ca<sup>2+</sup>, and Sr<sup>2+</sup>. Blue bars show Cs<sup>+</sup> removal efficiency (%) without competing ions (initial [Cs<sup>+</sup>] = ~1 ppm, adsorbent dose = 1.18 g L<sup>-1</sup>, and contact time = 5 h). (b) Ball and stick representation of pristine DGIST-3 (on left side) and Cs<sup>+</sup>@DGIST-3 (on right side), with dotted lines denoting ion—ion (dark green) and cation— $\pi$  (light green) interactions. Purple denotes Cs; green, In; yellow, O; gray, C; and blue, N. Hydrogen atoms are omitted for clarity.

sorbed the relatively soft  $Cs^+$  rather than the hard acidic cations. <sup>82,83</sup> Furthermore, because the cavities are properly sized,  $Cs^+$ , which has lower solvation energy than the other ions, accesses the cavities more easily than the other highly solvated hard cations. <sup>84</sup> For the same reason, divalent cations, accompanied by an additional anion, cannot be accommodated within the pores. Such selective affinity of the MOFs has not been exploited in other ion exchange sorbents that typically rely on ionic interactions. <sup>51,85–87</sup>

Adsorption Mechanism Studies. The Cs<sup>+</sup> adsorption mechanism was investigated by comparing the structures of DGIST-2, DGIST-3, and Cs<sup>+</sup>-containing DGIST-3 (denoted as Cs+@DGIST-3) determined by SXRD. In DGIST-2 and DGIST-3, the O-N distances (carboxylate to  $[Me_2NH_2]^+$ ) range from 3.63 to 3.73 Å and from 4.97 to 5.12 Å, respectively, which are longer than those of typical hydrogen bonds (Tables S4 and S6), 88 suggesting that [Me2NH2]+ ions interact weakly with the frameworks. 89 These [Me<sub>2</sub>NH<sub>2</sub>]<sup>+</sup> ions play a key role in the rapid Cs+ exchange. Furthermore, the cavity is sufficiently large that complete Cs<sup>+</sup> desolvation is not required, and thus, the sorption kinetics are not reduced. In addition, the flexible In(COO)<sub>4</sub> bonds and dangling naphthyl functional groups of DGIST-2'>methanol and DGIST-3 facilitate structural changes to accommodate Cs+ via multiple supramolecular interactions, including ion-ion (Cs+-In- $(COO)_4^-$ ) and cation- $\pi$  interactions  $(Cs^+$ -naphthalene) (Figure 4b). The unit cell parameters of pristine DGIST-3 are a = 18.057(4) Å, b = 20.023(4) Å, and c = 28.171(6) Å, while after Cs<sup>+</sup> adsorption, those for Cs<sup>+</sup>@DGIST-3 are a =18.223(4) Å, b = 19.640(4) Å, and c = 27.903(6) Å, accompanied by a unit cell volume reduction (10185(4) to 9986(3) Å<sup>3</sup>). In addition, the naphthyl-phenyl dihedral angle in L<sup>2-</sup> increased from 77.3° to 79.5°. As a result, the Cs-O3 and Cs-O2 bond lengths were 3.24 and 3.06 Å (Table S7), respectively, comparable to the Cs-O bond lengths found in previously reported anionic MOFs for Cs<sup>+</sup> sorption. <sup>49,81</sup> The distance between Cs+ and the neighboring aryl ring centroid was approximately 3.51 Å. This implies that cation  $-\pi$ interactions, 90,91 which were not observed between [Me<sub>2</sub>NH<sub>2</sub>]<sup>+</sup> ions and the framework in pristine DGIST-3, are involved in Cs<sup>+</sup> capture. Although cation  $-\pi$  interactions have been observed in diverse compounds, they are rarely exploited in cation adsorbents. 92,93

#### CONCLUSION

2D (DGIST-2) and 3D (DGIST-3) anionic MOFs with different arrangements of a naphthalimide-based ligand and  ${\rm In}^{3+}$  were synthesized and applied in the removal of Cs<sup>+</sup> from solutions. The phase transition of DGIST-2 in ethanol, methanol, and water resulted in the hydrolytic stability without compositional changes; the hydrophobic nature of the naphthyl group of the ligand, which is the major terminal site of the 2D crystal, presumably inhibits the ingress of water molecules. DGIST-3 exhibited a single-crystal-to-single-crystal transformation during Cs<sup>+</sup> capture, and structural analysis revealed multiple supramolecular interactions between the adsorbed Cs<sup>+</sup> and the framework, including ion—ion and cation— $\pi$  interactions that enable exceptionally rapid Cs<sup>+</sup> sorption.

## ASSOCIATED CONTENT

#### Supporting Information

The Supporting Information is available free of charge at https://pubs.acs.org/doi/10.1021/acs.inorgchem.1c03025.

Details for pH stability, contact angle, FT-NMR, FE-SEM with EDX, SXRD, PXRD, ICP-MS, IR, TGA, and EA data (PDF)

### **Accession Codes**

CCDC 2033459–2033460 and 2033525 contain the supplementary crystallographic data for this paper. These data can be obtained free of charge via www.ccdc.cam.ac.uk/data\_request/cif, or by emailing data\_request@ccdc.cam.ac.uk, or by contacting The Cambridge Crystallographic Data Centre, 12 Union Road, Cambridge CB2 1EZ, UK; fax: +44 1223 336033.

#### AUTHOR INFORMATION

## **Corresponding Authors**

Jinhee Park — Department of Emerging Materials Science, Daegu Gyeongbuk Institute of Science and Technology (DGIST), Dalseong-gun, Daegu 42988, Republic of Korea; orcid.org/0000-0001-7755-5889; Email: jinhee@dgist.ac.kr

Jian-Rong Li — Beijing Key Laboratory for Green Catalysis and Separation, Department of Chemistry and Chemical Engineering, College of Environmental and Energy Engineering, Beijing University of Technology, Beijing 100124, P. R. China; ⊚ orcid.org/0000-0002-8101-8493; Email: jrli@bjut.edu.cn

#### Authors

Kangwoo Jin – Department of Emerging Materials Science, Daegu Gyeongbuk Institute of Science and Technology (DGIST), Dalseong-gun, Daegu 42988, Republic of Korea

Xue-Qian Wu — Beijing Key Laboratory for Green Catalysis and Separation, Department of Chemistry and Chemical Engineering, College of Environmental and Energy Engineering, Beijing University of Technology, Beijing 100124, P. R. China

Ying-Pin Chen – NSF's ChemMatCARS, The University of Chicago, Argonne, Illinois 60439, United States

In-Hyeok Park – Graduate School of Analytical Science and Technology (GRAST), Chungnam National University, Daejeon 34134, Republic of Korea

Complete contact information is available at: https://pubs.acs.org/10.1021/acs.inorgchem.1c03025

#### **Notes**

The authors declare no competing financial interest.

## ACKNOWLEDGMENTS

This work was supported by the National Research Foundation (NRF) of Korea funded by the Ministry of Science and ICT (NRF-2019R1C1C1006058, NRF-2021R1A4A5030513, and NRF-2021M2D2A1A01039903) and the DGIST R&D Program of the Ministry of Science and ICT (20-HRHR-ET-09). NSF's ChemMatCARS Sector 15 is supported by the Divisions of Chemistry (CHE) and Materials Research (DMR), National Science Foundation, under grant number NSF/CHE-1834750. An Office of Science User Facility operated for the U.S. Department of Energy (DOE) Office of Science by Argonne National Laboratory was supported by the U.S. DOE under Contract No. DE-AC02-06CH11357.

#### REFERENCES

- (1) Murray, L. J.; Dincă, M.; Long, J. R. Hydrogen storage in metalorganic frameworks. *Chem. Soc. Rev.* **2009**, *38*, 1294–1314.
- (2) Connolly, B. M.; Madden, D. G.; Wheatley, A. E. H.; Fairen-Jimenez, D. Shaping the Future of Fuel: Monolithic Metal—Organic Frameworks for High-Density Gas Storage. *J. Am. Chem. Soc.* **2020**, 142, 8541–8549.
- (3) Zhao, X.; Wang, Y.; Li, D.-S.; Bu, X.; Feng, P. Metal-Organic Frameworks for Separation. *Adv. Mater.* **2018**, *30*, 1705189.
- (4) Xu, T.; Fan, L.; Jiang, Z.; Zhou, P.; Li, Z.; Lu, H.; He, Y. Immobilization of N-oxide functionality into NbO-type MOFs for significantly enhanced  $C_2H_2/CH_4$  and  $CO_2/CH_4$  separations. *Dalton Trans.* **2020**, 49, 7174–7181.
- (5) Xu, T.; Jiang, Z.; Liu, P.; Chen, H.; Lan, X.; Chen, D.; Li, L.; He, Y. Immobilization of Oxygen Atoms in the Pores of Microporous Metal—Organic Frameworks for C<sub>2</sub>H<sub>2</sub> Separation and Purification. *ACS Appl. Nano Mater.* **2020**, *3*, 2911–2919.
- (6) Jiang, Z.; Zou, Y.; Xu, T.; Fan, L.; Zhou, P.; He, Y. A hydrostable cage-based MOF with open metal sites and Lewis basic sites immobilized in the pore surface for efficient separation and purification of natural gas and C<sub>2</sub>H<sub>2</sub>. *Dalton Trans.* **2020**, 49, 3553—3561
- (7) Kreno, L. E.; Leong, K.; Farha, O. K.; Allendorf, M.; Van Duyne, R. P.; Hupp, J. T. Metal—Organic Framework Materials as Chemical Sensors. *Chem. Rev.* **2012**, *112*, 1105–1125.
- (8) Lustig, W. P.; Mukherjee, S.; Rudd, N. D.; Desai, A. V.; Li, J.; Ghosh, S. K. Metal—organic frameworks: functional luminescent and photonic materials for sensing applications. *Chem. Soc. Rev.* **2017**, *46*, 3242–3285.

- (9) Oliver, S. R. J. Cationic inorganic materials for anionic pollutant trapping and catalysis. *Chem. Soc. Rev.* **2009**, *38*, 1868–1881.
- (10) Desai, A. V.; Manna, B.; Karmakar, A.; Sahu, A.; Ghosh, S. K. A Water-Stable Cationic Metal—Organic Framework as a Dual Adsorbent of Oxoanion Pollutants. *Angew. Chem., Int. Ed.* **2016**, *55*, 7811—7815.
- (11) Pang, J.; Yuan, S.; Qin, J.-S.; Lollar, C. T.; Huang, N.; Li, J.; Wang, Q.; Wu, M.; Yuan, D.; Hong, M.; Zhou, H.-C. Tuning the Ionicity of Stable Metal—Organic Frameworks through Ionic Linker Installation. *J. Am. Chem. Soc.* **2019**, *141*, 3129–3136.
- (12) Furukawa, H.; Ko, N.; Go, Y. B.; Aratani, N.; Choi, S. B.; Choi, E.; Yazaydin, A. Ö.; Snurr, R. Q.; O'Keeffe, M.; Kim, J.; Yaghi, O. M. Ultrahigh Porosity in Metal-Organic Frameworks. *Science* **2010**, 329, 424–428.
- (13) Chen, Z.; Li, P.; Anderson, R.; Wang, X.; Zhang, X.; Robison, L.; Redfern, L. R.; Moribe, S.; Islamoglu, T.; Gómez-Gualdrón, D. A.; Yildirim, T.; Stoddart, J. F.; Farha, O. K. Balancing volumetric and gravimetric uptake in highly porous materials for clean energy. *Science* **2020**, *368*, 297–303.
- (14) Furukawa, H.; Cordova, K. E.; O'Keeffe, M.; Yaghi, O. M. The Chemistry and Applications of Metal-Organic Frameworks. *Science* **2013**, *341*, 1230444.
- (15) Collins, S. P.; Daff Thomas, D.; Piotrkowski Sarah, S.; Woo Tom, K. Materials design by evolutionary optimization of functional groups in metal-organic frameworks. *Sci. Adv.* **2016**, *2*, e1600954.
- (16) Kalmutzki, M. J.; Hanikel, N.; Yaghi Omar, M. Secondary building units as the turning point in the development of the reticular chemistry of MOFs. *Sci. Adv.* **2018**, *4*, eaat9180.
- (17) Kumar, P.; Pournara, A.; Kim, K.-H.; Bansal, V.; Rapti, S.; Manos, M. J. Metal-organic frameworks: Challenges and opportunities for ion-exchange/sorption applications. *Prog. Mater. Sci.* **2017**, *86*, 25–74.
- (18) He, H.; Hashemi, L.; Hu, M.-L.; Morsali, A. The role of the counter-ion in metal-organic frameworks' chemistry and applications. *Coord. Chem. Rev.* **2018**, *376*, 319–347.
- (19) Ma, L.; Yang, J.; Lu, B.-B.; Li, C.-P.; Ma, J.-F. Water-Stable Metal—Organic Framework for Effective and Selective  ${\rm Cr_2O_7}^{2-}$  Capture through Single-Crystal to Single-Crystal Anion Exchange. *Inorg. Chem.* **2018**, *57*, 11746–11752.
- (20) Zhang, J.; Chen, L.; Dai, X.; Zhu, L.; Xiao, C.; Xu, L.; Zhang, Z.; Alekseev, E. V.; Wang, Y.; Zhang, C.; Zhang, H.; Wang, Y.; Diwu, J.; Chai, Z.; Wang, S. Distinctive Two-Step Intercalation of Sr<sup>2+</sup> into a Coordination Polymer with Record High <sup>90</sup>Sr Uptake Capabilities. *Chem.* **2019**, *5*, 977–994.
- (21) Tian, D.; Wu, T.-T.; Liu, Y.-Q.; Li, N. Double-Walled Metal—Organic Framework with Regulable Pore Environments for Efficient Removal of Radioactive Cesium Cations. *Inorg. Chem.* **2021**, *60*, 12067–12074.
- (22) Dubchak, S. In *Impact of Cesium on Plants and the Environment*; Gupta, D. K., Walther, C., Eds.; Springer International Publishing: Cham, 2017; pp 1–18, DOI: 10.1007/978-3-319-41525-3\_1.
- (23) Namiki, Y.; Namiki, T.; Ishii, Y.; Koido, S.; Nagase, Y.; Tsubota, A.; Tada, N.; Kitamoto, Y. Inorganic-Organic Magnetic Nanocomposites for use in Preventive Medicine: A Rapid and Reliable Elimination System for Cesium. *Pharm. Res.* **2012**, 29, 1404—1418.
- (24) Goossens, R.; Delville, A.; Genot, J.; Halleux, R.; Masschelein, W. J. Removal of the typical isotopes of the chernobyl fall-out by conventional water treatment. *Water Res.* **1989**, *23*, 693–697.
- (25) Grüner, B.; Plešek, J.; Báča, J.; Francois Dozol, J.; Lamare, V.; Císařová, I.; Bělohradský, M.; Čáslavský, J. Crown ether substituted cobalta bis(dicarbollide) ions as selective extraction agents for removal of Cs<sup>+</sup> and Sr<sup>2+</sup> from nuclear waste. *New J. Chem.* **2002**, 26, 867–875.
- (26) Application of Ion Exchange Processes for Treatment of Radioactive Waste and Management of Spent Ion Exchangers; International Atomic Energy Agency: Vienna, 2002.
- (27) Yang, H.; Sun, L.; Zhai, J.; Li, H.; Zhao, Y.; Yu, H. In situ controllable synthesis of magnetic Prussian blue/graphene oxide

- nanocomposites for removal of radioactive cesium in water. *J. Mater. Chem. A* **2014**, *2*, 326–332.
- (28) Qi, X.-H.; Du, K.-Z.; Feng, M.-L.; Li, J.-R.; Du, C.-F.; Zhang, B.; Huang, X.-Y. A two-dimensionally microporous thiostannate with superior Cs<sup>+</sup> and Sr<sup>2+</sup> ion-exchange property. *J. Mater. Chem. A* **2015**, 3, 5665–5673.
- (29) Feng, M.-L.; Sarma, D.; Gao, Y.-J.; Qi, X.-H.; Li, W.-A.; Huang, X.-Y.; Kanatzidis, M. G. Efficient Removal of  $[UO_2]^{2+}$ ,  $Cs^+$ , and  $Sr^{2+}$  Ions by Radiation-Resistant Gallium Thioantimonates. *J. Am. Chem. Soc.* **2018**, *140*, 11133–11140.
- (30) Oancea, A. M. S.; Popescu, A. R.; Radulescu, M.; Weber, V.; Pincovschi, E.; Cox, M. Kinetics of Cesium and Strontium Ions Removal from Wastewater on Gel and Macroporous Resins. *Solvent Extr. Ion Exch.* **2008**, *26*, 217–239.
- (31) Prelot, B.; Ayed, I.; Marchandeau, F.; Zajac, J. On the real performance of cation exchange resins in wastewater treatment under conditions of cation competition: the case of heavy metal pollution. *Environ. Sci. Pollut. Res.* **2014**, *21*, 9334–9343.
- (32) Borai, E. H.; Harjula, R.; malinen, L.; Paajanen, A. Efficient removal of cesium from low-level radioactive liquid waste using natural and impregnated zeolite minerals. *J. Hazard. Mater.* **2009**, *172*, 416–422.
- (33) Kwon, S.; Kim, C.; Han, E.; Lee, H.; Cho, H. S.; Choi, M. Relationship between zeolite structure and capture capability for radioactive cesium and strontium. *J. Hazard. Mater.* **2021**, *408*, 124419
- (34) Datta, S. J.; Moon, W. K.; Choi, D. Y.; Hwang, I. C.; Yoon, K. B. A Novel Vanadosilicate with Hexadeca-Coordinated Cs<sup>+</sup> Ions as a Highly Effective Cs<sup>+</sup> Remover. *Angew. Chem., Int. Ed.* **2014**, *53*, 7203–7208.
- (35) Ding, N.; Kanatzidis, M. G. Selective incarceration of caesium ions by Venus flytrap action of a flexible framework sulfide. *Nat. Chem.* **2010**, *2*, 187–191.
- (36) Mertz, J. L.; Fard, Z. H.; Malliakas, C. D.; Manos, M. J.; Kanatzidis, M. G. Selective Removal of  $Cs^+$ ,  $Sr^{2+}$ , and  $Ni^{2+}$  by  $K_{2x}Mg_xSn_{3-x}S_6$  (x=0.5-1) (KMS-2) Relevant to Nuclear Waste Remediation. *Chem. Mater.* **2013**, 25, 2116–2127.
- (37) Manos, M. J.; Chrissafis, K.; Kanatzidis, M. G. Unique Pore Selectivity for Cs<sup>+</sup> and Exceptionally High NH<sub>4</sub><sup>+</sup> Exchange Capacity of the Chalcogenide Material K<sub>6</sub>Sn[Zn<sub>4</sub>Sn<sub>4</sub>S<sub>17</sub>]. *J. Am. Chem. Soc.* **2006**, *128*, 8875–8883.
- (38) Yang, H.; Luo, M.; Luo, L.; Wang, H.; Hu, D.; Lin, J.; Wang, X.; Wang, Y.; Wang, S.; Bu, X.; Feng, P.; Wu, T. Highly Selective and Rapid Uptake of Radionuclide Cesium Based on Robust Zeolitic Chalcogenide via Stepwise Ion-Exchange Strategy. *Chem. Mater.* **2016**, *28*, 8774–8780.
- (39) Park, Y.; Lee, Y.-C.; Shin, W. S.; Choi, S.-J. Removal of cobalt, strontium and cesium from radioactive laundry wastewater by ammonium molybdophosphate—polyacrylonitrile (AMP—PAN). *Chem. Eng. J.* **2010**, *162*, 685–695.
- (40) Ding, D.; Zhang, Z.; Chen, R.; Cai, T. Selective removal of cesium by ammonium molybdophosphate polyacrylonitrile bead and membrane. *J. Hazard. Mater.* **2017**, 324, 753–761.
- (41) Poojary, D. M.; Cahill, R. A.; Clearfield, A. Synthesis, Crystal Structures, and Ion-Exchange Properties of a Novel Porous Titanosilicate. *Chem. Mater.* **1994**, *6*, 2364–2368.
- (42) Zheng, Z.; Philip, C. V.; Anthony, R. G.; Krumhansl, J. L.; Trudell, D. E.; Miller, J. E. Ion Exchange of Group I Metals by Hydrous Crystalline Silicotitanates. *Ind. Eng. Chem. Res.* **1996**, *35*, 4246–4256.
- (43) Celestian, A. J.; Kubicki, J. D.; Hanson, J.; Clearfield, A.; Parise, J. B. The Mechanism Responsible for Extraordinary Cs Ion Selectivity in Crystalline Silicotitanate. *J. Am. Chem. Soc.* **2008**, *130*, 11689–11694.
- (44) Petersková, M.; Valderrama, C.; Gibert, O.; Cortina, J. L. Extraction of valuable metal ions (Cs, Rb, Li, U) from reverse osmosis concentrate using selective sorbents. *Desalination* **2012**, 286, 316–323.

- (45) Chen, G.-R.; Chang, Y.-R.; Liu, X.; Kawamoto, T.; Tanaka, H.; Kitajima, A.; Parajuli, D.; Takasaki, M.; Yoshino, K.; Chen, M.-L.; Lo, Y.-K.; Lei, Z.; Lee, D.-J. Prussian blue (PB) granules for cesium (Cs) removal from drinking water. *Sep. Purif. Technol.* **2015**, *143*, 146–151.
- (46) Wang, L.; Pei, H.; Sarma, D.; Zhang, X.-M.; MacRenaris, K.; Malliakas, C. D.; Kanatzidis, M. G. Highly Selective Radioactive <sup>137</sup>Cs<sup>+</sup> Capture in an Open-Framework Oxysulfide Based on Supertetrahedral Cluster. *Chem. Mater.* **2019**, *31*, 1628–1634.
- (47) Liao, Y.-Y.; Li, J.-R.; Zhang, B.; Sun, H.-Y.; Ma, W.; Jin, J.-C.; Feng, M.-L.; Huang, X.-Y. Robust and Flexible Thioantimonate Materials for Cs<sup>+</sup> Remediation with Distinctive Structural Transformation: A Clear Insight into the Ion-Exchange Mechanism. *ACS Appl. Mater. Interfaces* **2021**, *13*, 5275–5283.
- (48) Manos, M. J.; Kanatzidis, M. G. Highly Efficient and Rapid  $Cs^+$  Uptake by the Layered Metal Sulfide  $K_{2x}Mn_xSn_{3-x}S_6$  (KMS-1). *J. Am. Chem. Soc.* **2009**, *131*, 6599–6607.
- (49) Gao, Y.-J.; Feng, M.-L.; Zhang, B.; Wu, Z.-F.; Song, Y.; Huang, X.-Y. An easily synthesized microporous framework material for the selective capture of radioactive Cs<sup>+</sup> and Sr<sup>2+</sup> ions. *J. Mater. Chem. A* **2018**, *6*, 3967–3976.
- (50) Wang, Y.; Liu, Z.; Li, Y.; Bai, Z.; Liu, W.; Wang, Y.; Xu, X.; Xiao, C.; Sheng, D.; Diwu, J.; Su, J.; Chai, Z.; Albrecht-Schmitt, T. E.; Wang, S. Umbellate Distortions of the Uranyl Coordination Environment Result in a Stable and Porous Polycatenated Framework That Can Effectively Remove Cesium from Aqueous Solutions. *J. Am. Chem. Soc.* **2015**, *137*, 6144–6147.
- (51) Aguila, B.; Banerjee, D.; Nie, Z.; Shin, Y.; Ma, S.; Thallapally, P. K. Selective removal of cesium and strontium using porous frameworks from high level nuclear waste. *Chem. Commun.* **2016**, 52, 5940–5942.
- (52) Rapti, S.; Pournara, A.; Sarma, D.; Papadas, I. T.; Armatas, G. S.; Tsipis, A. C.; Lazarides, T.; Kanatzidis, M. G.; Manos, M. J. Selective capture of hexavalent chromium from an anion-exchange column of metal organic resin—alginic acid composite. *Chem. Sci.* **2016**, *7*, 2427–2436.
- (53) Howarth, A. J.; Liu, Y.; Li, P.; Li, Z.; Wang, T. C.; Hupp, J. T.; Farha, O. K. Chemical, thermal and mechanical stabilities of metalorganic frameworks. *Nat. Rev. Mater.* **2016**, *1*, 15018.
- (54) Senker, J. Crumple zones in MOFs. *Nat. Chem.* **2018**, *10*, 1079–1081.
- (55) Ding, M.; Cai, X.; Jiang, H.-L. Improving MOF stability: approaches and applications. *Chem. Sci.* **2019**, *10*, 10209–10230.
- (56) Nguyen, J. G.; Cohen, S. M. Moisture-Resistant and Superhydrophobic Metal—Organic Frameworks Obtained via Postsynthetic Modification. *J. Am. Chem. Soc.* **2010**, *132*, 4560–4561.
- (57) Yuan, S.; Feng, L.; Wang, K.; Pang, J.; Bosch, M.; Lollar, C.; Sun, Y.; Qin, J.; Yang, X.; Zhang, P.; Wang, Q.; Zou, L.; Zhang, Y.; Zhang, L.; Fang, Y.; Li, J.; Zhou, H.-C. Stable Metal—Organic Frameworks: Design, Synthesis, and Applications. *Adv. Mater.* **2018**, 30, 1704303.
- (58) Jayaramulu, K.; Geyer, F.; Schneemann, A.; Kment, Ś.; Otyepka, M.; Zboril, R.; Vollmer, D.; Fischer, R. A. Hydrophobic Metal—Organic Frameworks. *Adv. Mater.* **2019**, *31*, 1900820.
- (59) Isaka, Y.; Kawase, Y.; Kuwahara, Y.; Mori, K.; Yamashita, H. Two-Phase System Utilizing Hydrophobic Metal—Organic Frameworks (MOFs) for Photocatalytic Synthesis of Hydrogen Peroxide. *Angew. Chem., Int. Ed.* **2019**, *58*, 5402–5406.
- (60) Reger, D. L.; Leitner, A. P.; Smith, M. D. Supramolecular Metal—Organic Frameworks of s- and f-Block Metals: Impact of 1,8-Naphthalimide Functional Group. *Cryst. Growth Des.* **2016**, *16*, 527–536.
- (61) Liu, J.-J.; Xia, S.-B.; Que, Q.-T.; Suo, H.; Liu, J.; Shen, X.; Cheng, F.-X. Naphthalimide-containing coordination polymer with mechanoresponsive luminescence and excellent metal ion sensing properties. *Dalton Trans.* **2020**, *49*, 3174–3180.
- (62) Kirdponpattara, S.; Phisalaphong, M.; Newby, B.-m. Z. Applicability of Washburn capillary rise for determining contact angles of powders/porous materials. *J. Colloid Interface Sci.* **2013**, 397, 169–176.

- (63) Yuan, B.; Yin, X.-Q.; Liu, X.-Q.; Li, X.-Y.; Sun, L.-B. Enhanced Hydrothermal Stability and Catalytic Performance of HKUST-1 by Incorporating Carboxyl-Functionalized Attapulgite. *ACS Appl. Mater. Interfaces* **2016**, *8*, 16457–16464.
- (64) Jayaramulu, K.; Datta, K. K. R.; Rösler, C.; Petr, M.; Otyepka, M.; Zboril, R.; Fischer, R. A. Biomimetic Superhydrophobic/Superoleophilic Highly Fluorinated Graphene Oxide and ZIF-8 Composites for Oil–Water Separation. *Angew. Chem., Int. Ed.* **2016**, 55, 1178–1182.
- (65) DeChellis, D. M.; Ngule, C. M.; Genna, D. T. Removal of hydrocarbon contaminants from water with perfluorocarboxylated UiO-6X derivatives. *J. Mater. Chem. A* **2020**, *8*, 5848–5852.
- (66) Liu, Y.; Eubank, J. F.; Cairns, A. J.; Eckert, J.; Kravtsov, V. C.; Luebke, R.; Eddaoudi, M. Assembly of Metal—Organic Frameworks (MOFs) Based on Indium-Trimer Building Blocks: A Porous MOF with soc Topology and High Hydrogen Storage. *Angew. Chem., Int. Ed.* **2007**, *46*, 3278–3283.
- (67) Zheng, S.-T.; Bu, J. T.; Li, Y.; Wu, T.; Zuo, F.; Feng, P.; Bu, X. Pore Space Partition and Charge Separation in Cage-within-Cage Indium—Organic Frameworks with High CO<sub>2</sub> Uptake. *J. Am. Chem. Soc.* **2010**, *132*, 17062–17064.
- (68) Gándara, F.; Gomez-Lor, B.; Gutiérrez-Puebla, E.; Iglesias, M.; Monge, M. A.; Proserpio, D. M.; Snejko, N. An Indium Layered MOF as Recyclable Lewis Acid Catalyst. *Chem. Mater.* **2008**, *20*, 72–76.
- (69) Zheng, S.-T.; Bu, J. J.; Wu, T.; Chou, C.; Feng, P.; Bu, X. Porous Indium—Organic Frameworks and Systematization of Structural Building Blocks. *Angew. Chem., Int. Ed.* **2011**, *50*, 8858—8862
- (70) Zhang, B.; Zhang, S.-H.; Liu, B.; Yue, K.-F.; Hou, L.; Wang, Y.-Y. Stable Indium-Pyridylcarboxylate Framework: Selective Gas Capture and Sensing of Fe<sup>3+</sup> Ion in Water. *Inorg. Chem.* **2018**, *57*, 15262–15269.
- (71) Zhong, W.-B.; Li, R.-X.; Lv, J.; He, T.; Xu, M.-M.; Wang, B.; Xie, L.-H.; Li, J.-R. Two isomeric In(iii)-MOFs: unexpected stability difference and selective fluorescence detection of fluoroquinolone antibiotics in water. *Inorg. Chem. Front.* **2020**, *7*, 1161–1171.
- (72) Yu, P.; Li, Q.; Hu, Y.; Liu, N.; Zhang, L.; Su, K.; Qian, J.; Huang, S.; Hong, M. Cuboctahedron-based indium—organic frameworks for gas sorption and selective cation exchange. *Chem. Commun.* **2016**, *52*, 7978—7981.
- (73) Joarder, B.; Lin, J.-B.; Romero, Z.; Shimizu, G. K. H. Single Crystal Proton Conduction Study of a Metal Organic Framework of Modest Water Stability. *J. Am. Chem. Soc.* **2017**, *139*, 7176–7179.
- (74) Peng, Y.-W.; Wu, R.-J.; Liu, M.; Yao, S.; Geng, A.-F.; Zhang, Z.-M. Nitrogen Coordination To Dramatically Enhance the Stability of In-MOF for Selectively Capturing CO<sub>2</sub> from a CO<sub>2</sub>/N<sub>2</sub> Mixture. *Cryst. Growth Des.* **2019**, *19*, 1322–1328.
- (75) Liu, L.; Zhang, X.-N.; Han, Z.-B.; Gao, M.-L.; Cao, X.-M.; Wang, S.-M. An In<sup>III</sup>-based anionic metal—organic framework: sensitization of lanthanide (III) ions and selective absorption and separation of cationic dyes. *J. Mater. Chem. A* **2015**, *3*, 14157–14164.
- (76) Zou, L.; Sun, X.; Yuan, J.; Li, G.; Liu, Y. Assembly of Zeolite-like Metal—Organic Framework: An Indium-ZMOF Possessing GIS Topology and High CO<sub>2</sub> Capture. *Inorg. Chem.* **2018**, *57*, 10679—10684.
- (77) Li, G.; Ji, G.; Liu, W.; Zhang, J.; Song, L.; Cheng, L.; Wang, X.; Wang, Y.; Liu, J.; Chen, X.; Sun, X.; Diwu, J. A hydrolytically stable anionic layered indium—organic framework for the efficient removal of <sup>90</sup>Sr from seawater. *Dalton Trans.* **2019**, *48*, 17858–17863.
- (78) Fan, L.; Zhou, P.; Wang, X.; Yue, L.; Li, L.; He, Y. Rational Construction and Performance Regulation of an In(III)—Tetraisophthalate Framework for One-Step Adsorption-Phase Purification of C<sub>2</sub>H<sub>4</sub> from C<sub>2</sub> Hydrocarbons. *Inorg. Chem.* **2021**, *60*, 10819–10829.
- (79) Makal, T. A.; Yakovenko, A. A.; Zhou, H.-C. Isomerism in Metal-Organic Frameworks: "Framework Isomers. *J. Phys. Chem. Lett.* **2011**, *2*, 1682–1689.
- (80) Ho, Y.-S. Review of second-order models for adsorption systems. J. Hazard. Mater. 2006, 136, 681-689.

- (81) Ai, J.; Chen, F.-Y.; Gao, C.-Y.; Tian, H.-R.; Pan, Q.-J.; Sun, Z.-M. Porous Anionic Uranyl—Organic Networks for Highly Efficient Cs<sup>+</sup> Adsorption and Investigation of the Mechanism. *Inorg. Chem.* **2018**, *57*, 4419–4426.
- (82) James, A. M.; Harding, S.; Robshaw, T.; Bramall, N.; Ogden, M. D.; Dawson, R. Selective Environmental Remediation of Strontium and Cesium Using Sulfonated Hyper-Cross-Linked Polymers (SHCPs). ACS Appl. Mater. Interfaces 2019, 11, 22464—22473.
- (83) Zhu, D.; Herbert, B. E.; Schlautman, M. A.; Carraway, E. R.; Hur, J. Cation— $\pi$  Bonding: A New Perspective on the Sorption of Polycyclic Aromatic Hydrocarbons to Mineral Surfaces. *J. Environ. Qual.* **2004**, *33*, 1322–1330.
- (84) Selegue, T. J.; Moe, N.; Draves, J. A.; Lisy, J. M. Gas phase solvation of Na<sup>+</sup> with methanol. *J. Chem. Phys.* **1992**, *96*, 7268–7278.
- (85) Ding, D.; Zhao, Y.; Yang, S.; Shi, W.; Zhang, Z.; Lei, Z.; Yang, Y. Adsorption of cesium from aqueous solution using agricultural residue Walnut shell: Equilibrium, kinetic and thermodynamic modeling studies. *Water Res.* **2013**, *47*, 2563–2571.
- (86) Olatunji, M. A.; Khandaker, M. U.; Mahmud, H. N. M. E.; Amin, Y. M. Influence of adsorption parameters on cesium uptake from aqueous solutions- a brief review. *RSC Adv.* **2015**, *5*, 71658–71683.
- (87) Han, E.; Kim, Y.-G.; Yang, H.-M.; Yoon, I.-H.; Choi, M. Synergy between Zeolite Framework and Encapsulated Sulfur for Enhanced Ion-Exchange Selectivity to Radioactive Cesium. *Chem. Mater.* **2018**, *30*, 5777–5785.
- (88) Steiner, T. The Hydrogen Bond in the Solid State. Angew. Chem., Int. Ed. 2002, 41, 48-76.
- (89) Su, J.; Yuan, S.; Wang, H.-Y.; Huang, L.; Ge, J.-Y.; Joseph, E.; Qin, J.; Cagin, T.; Zuo, J.-L.; Zhou, H.-C. Redox-switchable breathing behavior in tetrathiafulvalene-based metal—organic frameworks. *Nat. Commun.* **2017**, *8*, 2008.
- (90) Lenthall, J. T.; Steed, J. W. Organometallic cavitands: Cation $-\pi$  interactions and anion binding via  $\pi$ -metallation. *Coord. Chem. Rev.* **2007**, 251, 1747–1760.
- (91) Kumari, H.; Jin, P.; Teat, S. J.; Barnes, C. L.; Dalgarno, S. J.; Atwood, J. L. Strong Cation $\cdots\pi$  Interactions Promote the Capture of Metal Ions within Metal-Seamed Nanocapsule. *J. Am. Chem. Soc.* **2014**, 136, 17002–17005.
- (92) Mahadevi, A. S.; Sastry, G. N. Cation— $\pi$  Interaction: Its Role and Relevance in Chemistry, Biology, and Material Science. *Chem. Rev.* **2013**, *113*, 2100–2138.
- (93) Wei, X.; Kang, X.; Yuan, Q.; Qin, C.; Jin, S.; Wang, S.; Zhu, M. Capture of Cesium Ions with Nanoclusters: Effects on Inter- and Intramolecular Assembly. *Chem. Mater.* **2019**, *31*, 4945–4952.